BioNanoScience (2019) 9:164–171
https://doi.org/10.1007/s12668-018-0579-3

Biosynthesis and Cytotoxic Study of Synthesized Zinc Oxide Nanoparticles Using *Salvadora persica*

Abdolhossein Miri [1] · **Mina Sarani** [2,3]

Published online: 29 November 2018

Abstract
Salvadora persica extract was utilized as a mediate in the synthesis of zinc oxide nanoparticles (ZnO-NPs) under ambient conditions. The biosynthesized particles were characterized via UV-Vis, PXRD, FESEM, EDX, DLS, Raman, and FT-IR analysis. The UV-Vis studies of these particular nanoparticles revealed a characteristic peak at 383 nm, and PXRD pattern presented wurtzite structure (hexagonal) for the synthesized ZnO-NPs, suggesting the formation of ZnO nanoparticles. The FESEM image indicated that the biosynthesized particles were uniformly shaped in hexagonal with the average size of 60–130 nm at calcination temperatures of 500, 600, and 700 °C. On the other hand, the EDX clearly exhibited the presence of Zn and O elements in the biosynthesized sample. The powder x-ray diffraction (PXRD) and Raman studies confirmed the formation of single crystalline, hexagonal wurtzite ZnO structures. The cytotoxic activity of the biosynthesized nanoparticles against HT-29 cancer cell line was examined through MTT assay. The results indicated that the toxicity of synthesized nanoparticles is dependent on the concentration of nanoparticles.

Keywords ZnO-NPs · *Salvadora persica* · Raman · MTT assay · HT-29

1 Introduction

Zinc oxide nanoparticles (ZnO-NPs) stand as significant nanoscale inorganic materials with a broad range of applications, as they have shown low toxicity at optimal concentrations and have been used as a trace element in the metabolism process. Their other usages include photocatalysis to eliminate environmental contaminants. Since ZnO-NPs are safe and environmentally friendly particles, they are widely utilized in cosmetic industries, ceramics, rubber, electronics, sensors, electrodes, and medical industry. Nanoparticles can easily cross the cell membrane and manipulate the cell cycles, leading to the disruption of cellular homeostasis [1]; therefore, they can be a suitable candidate for cancer treatment. ZnO-NPs can stand as a promising anticancer agent due to their unique properties such as biocompatibility, excellent selectivity, and easily fabricated [2]. The excess concentration of zinc is severely harmful for cells since it changes the metabolism and interrupts structures of DNA and proteins. Wahab et al. demonstrated that the cytotoxic effect of ZnO-NPs depended on the concentration of nanoparticles against MCF-7 and HepG2 cell lines. They also suggested that agglomeration of nanoparticles ($\sim 13 \pm 2$ nm) in cytoplasm can lead to damaged cellular organelles such as DNA, RNA, and mitochondria [3].

Typical ZnO-NPs production methods include the vapor phase process in the presence of a metal catalyst, thermal evaporation, sol-gel, and hydrothermal techniques. However, these procedures are not cost-effective and seem to cause contamination [4]. As a simple and less expensive method, the biosynthesis of nanoparticles has been a great innovation in recent years. Meanwhile, plant ingredients have the potential of acting as capper and reducer agents for metal ions [4–11].

Salvadora grows widely in tropical and subtropical regions of Africa and Asia, which is also capable of well adapting itself in saline lands [12]. Studies have reported that its compounds include terpenoids, non-volatile oils,

✉ Mina Sarani
minasarani64@gmail.com; m.sarani@zbmu.ac.ir

[1] Department of Pharmacognosy, Faculty of Pharmacy, Zabol University of Medical Sciences, Zabol, Iran

[2] NanoBioEletrochemistry Research Center, Bam University of Medical Sciences, Bam, Iran

[3] Student Research Committee, School of Medicine, Bam University of Medical Sciences, Bam, Iran

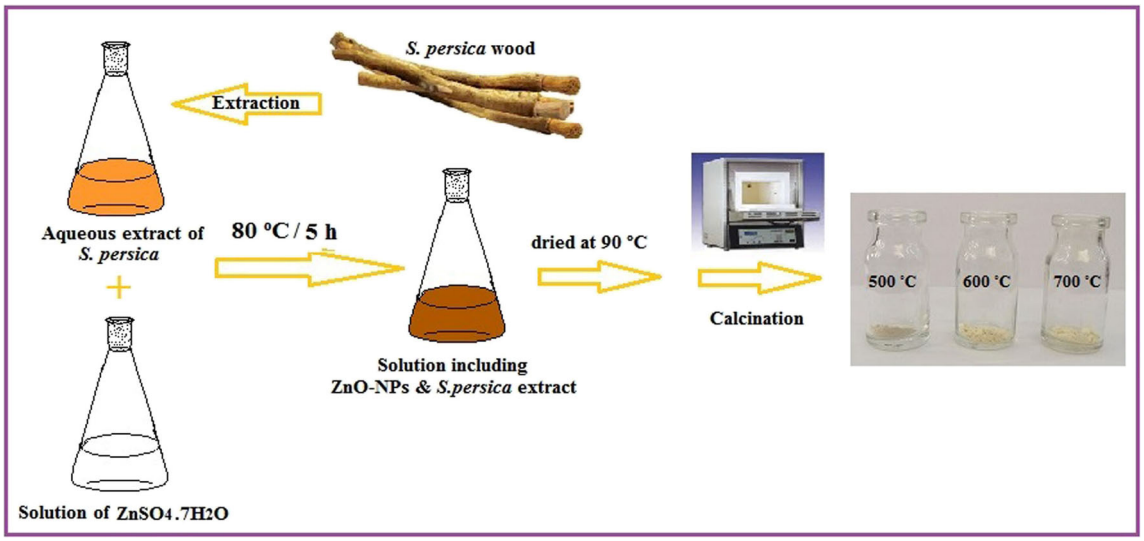

Fig. 1 Schematic plan of synthesized ZnO-NPs using aqueous extract of *S. persica*

steroids, alkaloids, flavonoids, saponins, and tannins [13]. *Salvadora persica* is a cosmopolite herb that has been utilized in traditional medicine for cleaning, whitening and polishing teeth, eliminating bad breath, strengthening gums, resolving inflammation of the body, reducing eye tears, increasing vision and eliminating blurred vision, enhancing appetite, fast treatment of constipation, and strengthening memory [14–17]. Based on previous studies, the accumulation of ZnO-NPs in the cells results in the destruction of cellular organs and the death of cells; therefore, these nanoparticles have potential for cancer treatment, so after the biosynthesis of ZnO-NPs using *S. persica* plant, its toxicity effects was investigated against colon (HT-29) cancer cell line.

2 Materials and Methods

2.1 Materials and Reagents

Salvatodra persica wood was collected from Khash, Sistan and Baluchestan, Iran. They were cleaned and dried at ambient temperature and gradually grounded and stored for further studies. Distilled water was used as solvent. Zinc sulfate ($ZnSO_4.7H_2O$) was purchased from Merck (Germany) and colon (HT-29) cancer cell line was attained from Pasteur Institute of Iran. The cells were incubated in RPMI media with FBS 10%, 100 μg/ml of streptomycin, and 100 U/ml of penicillin, at a temperature of 37 °C and the atmosphere of CO_2 with moisture 5%.

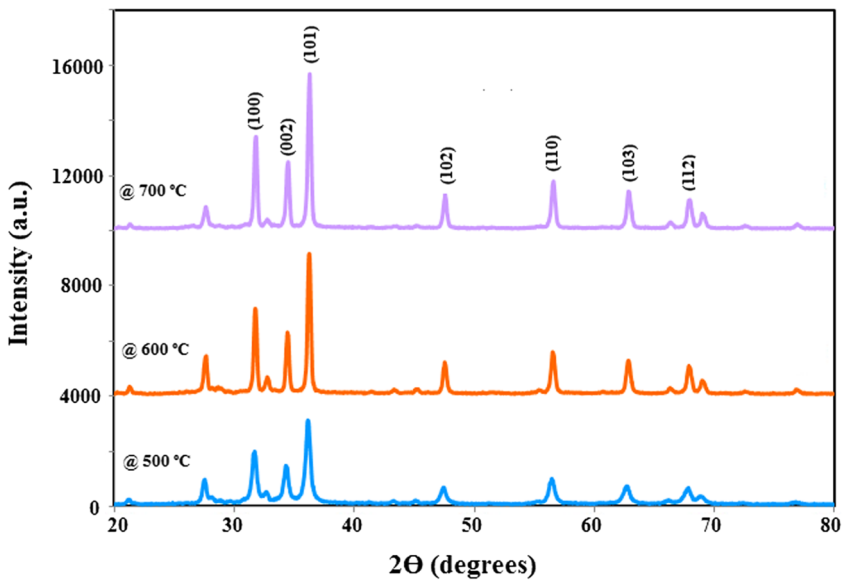

Fig. 2 PXRD diagrams of synthesized ZnO-NPs applying *S. persica* at different temperatures

2.2 Preparation of *S. persica* Extract

The aqueous extract of wood of tree branches of *S. persica* was prepared through the maceration method, which involved using distilled water (1 g:10 mL ratio) and a shaking process at 150 rpm for 5 h. The mixture was filtered through Whatman paper number 1, with the obtained filtrate brown solution kept at 4–7 °C.

2.3 Synthesis of ZnO-NPs

The volume of aqueous extract of *S. persica* (5 mL) was brought to 50 mL by distilled water and then was added to 50 mL of aqueous zinc sulfate solution (3 mM). The mixture was stirred at 80 °C for a period of 5 h and afterwards, the solvent was dried at 90 °C. The residue was placed in a furnace at 500, 600, and 700 °C separately for 2 h. The resulting white powder was characterized and identified to be ZnO-NPs.

2.4 Characterization of ZnO-NPs

The crystalline structure of the prepared ZnO-NPs was determined by powder x-ray diffraction (PXRD, X'Pert PRO MPD PANalytical Company, Netherlands). UV-Vis studies on the nanoparticles were conducted via UV-Vis spectrophotometer

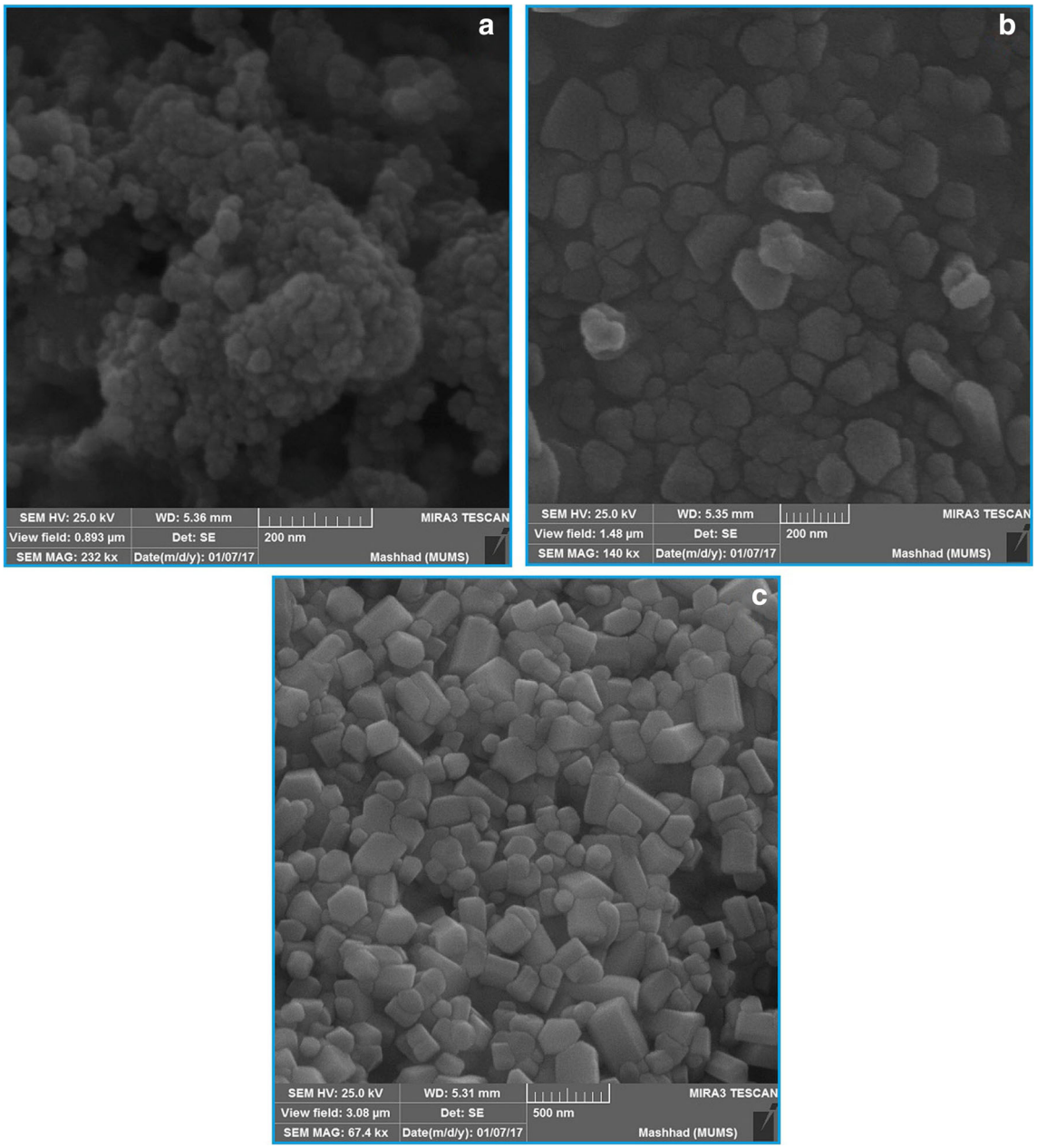

Fig. 3 FESEM images of synthesized ZnO-NPs using *S. persica* at the temperatures of (**a**) 500, (**b**) 600, and (**c**) 700 °C

(Rayleighuv-2100 model, China). Particle size analysis of synthesized nanoparticles was done by using DLS (dynamic light scattering, Malvern, ZEN3600, UK). The field emission scanning electron microscopy (FESEM) of ZnO-NPs was recorded by employing MIRA3 TESCAN.

2.5 Cytotoxicity Evaluation of ZnO-NPs

The cytotoxic activity of synthesized ZnO-NPs was evaluated using 3-(4,5-dimethylthiazol-2-yl)-2,5-diphenyltetrazolium bromide (MTT). Briefly, 200 μL of cell suspension was poured into a 96-well tissue culture plate (1×10^4 cell/well) and incubated for 24 h at 37 °C. Then, 50 μL of the synthesized nanoparticles (500, 250, 125, 62.5, and 13.25 μg/mL, separately) was added into each well and incubated for 24 h. The cell suspension with culture medium marked as the control. Afterwards, 20 μL of the PBS buffer which contained MTT (5 mg/mL) was appended to each well while the plates were incubated for 3 h at 37 °C. At the end, 100 μL of DMSO was added to each well and their optical absorbances were measured to be at 570 nm using a micro-plate reader. Cell viability was expressed as a percentage relative to the control.

2.6 Statistical Analysis

GraphPad Prism 5 was employed for statistical analysis with each value presented as mean ± SD. The statistical comparisons of multi-group data were analyzed through the usage of two-way ANOVA, with $*p < 0.001$ considered as statistically significant. All of the mentioned tests were performed in triplicates.

3 Results and Discussion

Nanoparticles are usually prepared via the reduction of metal ions and oxides using electron-donating agents such as water-soluble metal salts, hydrogen gas (H_2), borohydride salts (ABH_4), hydrazine (N_2H_4), organic acids (carboxylic acids), and many different alcohols. These agents are often toxic and expensive. Researches have revealed that the ingredients of plants, such as phenolic compounds and sugars, simply donate their electron constituting the very basis of green synthesis of nanoparticles. The wood of *S. persica* is known to be rich in flavonoids and tannins. They are well reductant and have been applied in the synthesis of metal oxide nanoparticles. Hence, the substrate of this plant has been utilized for the synthesis of ZnO-NPs (Fig. 1).

The PXRD patterns of the synthesized ZnO-NPs are illustrated in Fig. 2. All of the peaks have been specified by Miller indices including (100), (002), (101), (102), (110), (103), (200), (112), (201), (004), and (202), which can refer to the wurtzite structure (hexagonal) for synthesized ZnO-NPs [18, 19]. The effect of calcination temperature (500, 600, and 700 °C) was investigated on synthesized nanoparticles. Comparisons between the calcination temperatures revealed that similar crystals have been produced. It was observed in the PXRD graphs of three different temperatures that by increasing the calcination temperature, PXRD peaks became sharper and FWHM diminished (Fig. 2). This suggests that

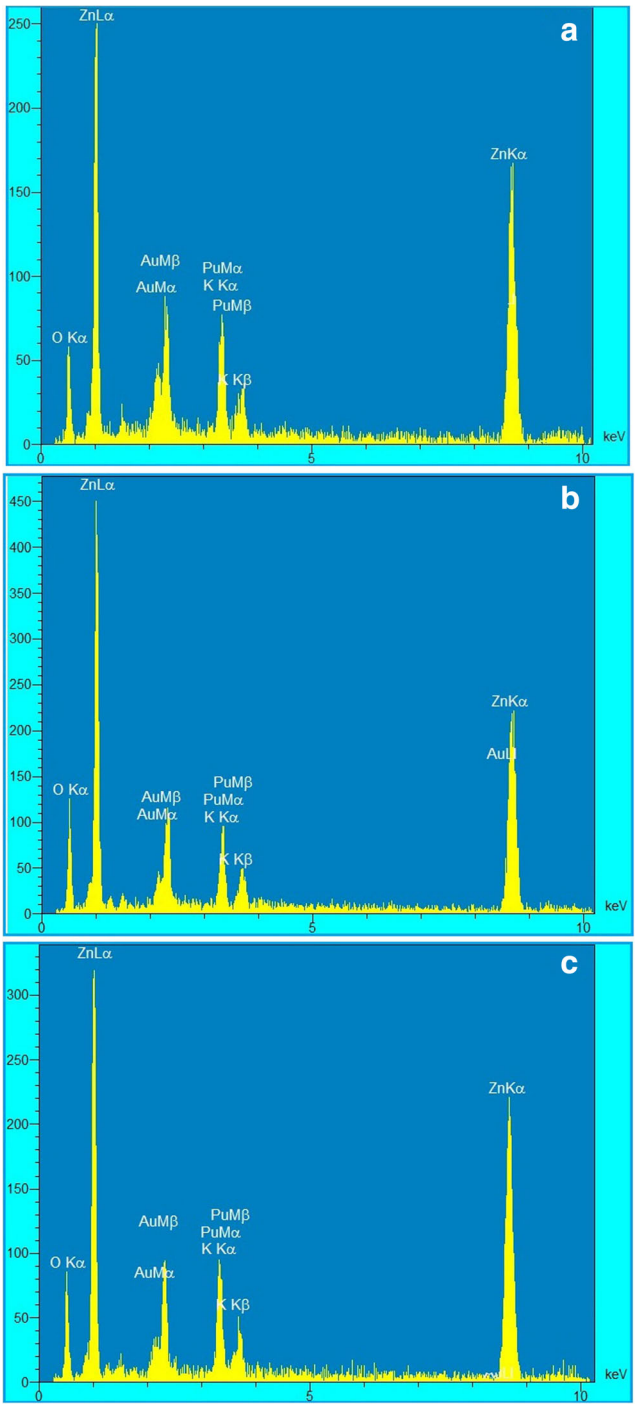

Fig. 4 EDX images of synthesized ZnO-NPs using *S. persica* at the temperatures of (**a**) 500, (**b**) 600, and (**c**) 700 °C

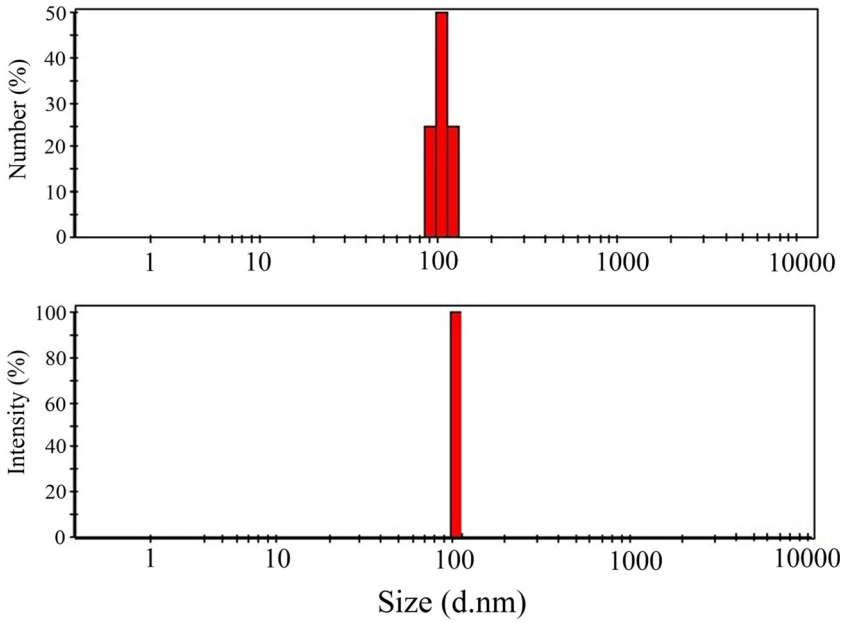

Fig. 5 Size distribution of synthesized ZnO-NPs with *S. persica* at 600 °C

the crystallization of nanoparticles can be accelerated by elevating the calcination temperature.

The FESEM images of the synthesized ZnO-NPs at 500, 600, and 700 °C are presented in Fig. 3. The images show that the ZnO particles are hexagonal and uniform in shape, with their size calculated as about 60–130 nm (Fig. 3). Riyadh M. Alwan et al. stated that ZnO-NPs grow after their synthesis, even when they are stored at room temperature. The synthesized ZnO-NPs have been observed to have spherical shapes and sizes of 100–200 nm [20]. P. Rajiv et al. was synthesized ZnO-NPs in different sizes by using *Parthenium hysterophorus* L. extract. They showed a size-dependent activity for antifungal properties of ZnO-NPs against plant fungal pathogens and stated that size change of particles can affect on properties of particles, directly [21]. The chemical composition of the synthesized nanoparticles was examined by EDX, showing only the presence of zinc and oxygen atoms at 500, 600, and 700 °C, representing the high purity of synthesized nanoparticles (Fig. 4). According to the spectra, the weight percentage of zinc and oxygen atoms was 63.75% and 22.00% at 500 °C, 67.46% and 22.91% at 600 °C, and 64.06% and 20.75% at 700 °C.

The particle size distribution was measured for the synthesized nanoparticles at 600 °C through dynamic light scattering (DLS) technique. As shown in Fig. 5, the size of synthesized nanoparticles is in the range of 105 nm, which it is according to SEM results.

The results indicated that ZnO-NPs were synthesized within a short timing process with high purity. The electronic spectrum of synthesized nanoparticles at 600 °C has shown an absorption peak at 383 nm (Fig. 6). This absorption band can be intrinsic to the band-gap of ZnO arising from an electron transfer from the valence to conduction band ($Zn_3d \rightarrow O_2p$) [22, 23].

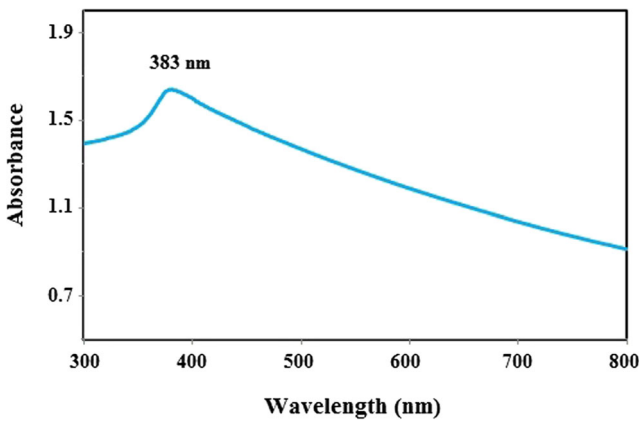

Fig. 6 UV-Vis spectrum of synthesized ZnO-NPs with *S. persica* at 600 °C

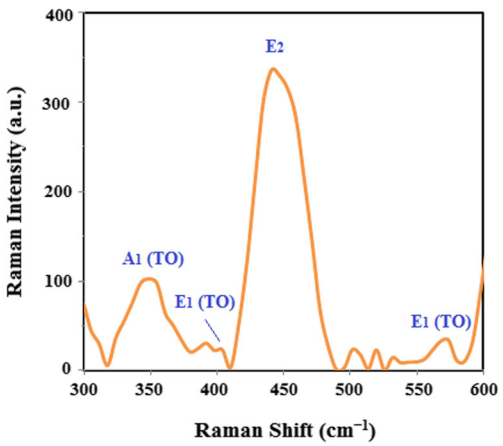

Fig. 7 Raman spectrum of synthesized ZnO-NPs at 600 °C

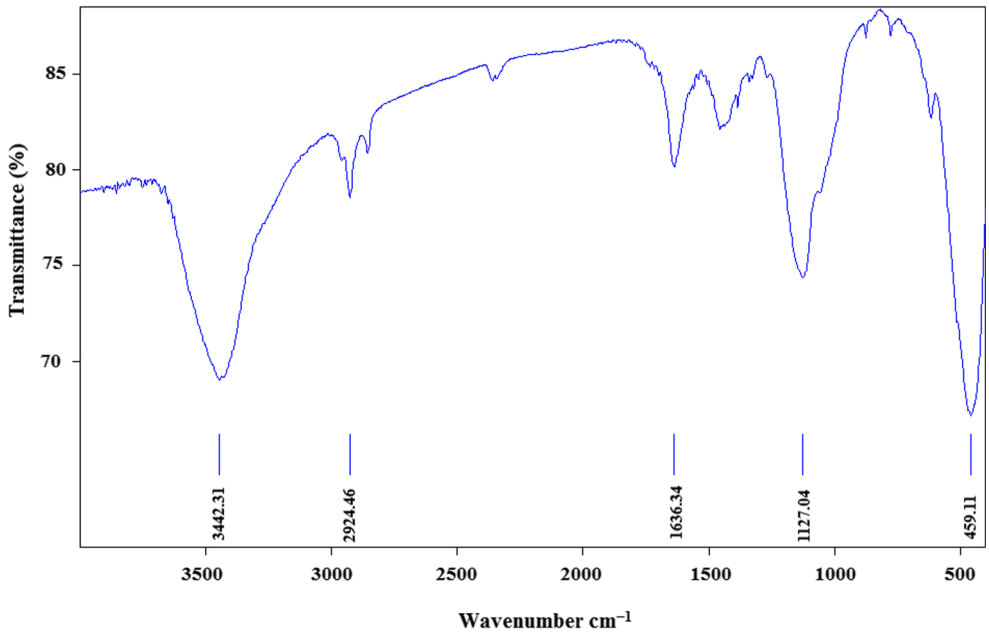

Fig. 8 FT-IR spectrum of synthesized ZnO-NPs using *S. persica* at 600 °C

The Raman spectrum of synthesized ZnO has revealed a sharp peak at 441 cm^{-1}, at the calcination temperature of 600 °C, corresponding to the hexagonal ZnO optical phonon E_2 mode (Fig. 7). According to the Raman, the synthesized nanoparticles contain a hexagonal structure belonging to the space group of C^4_{6v} [24], while its optical phonons belong to the following irreducible representations: $\Gamma_{opt} = A_1 + 2B_1 + E_1 + 2E_2$. A_1, E_1, and E_2 modes are Raman active, and the polar modes of A_1 and E_1 would be the infrared active splitting into transverse (TO) and longitudinal (LO) phonos [25].

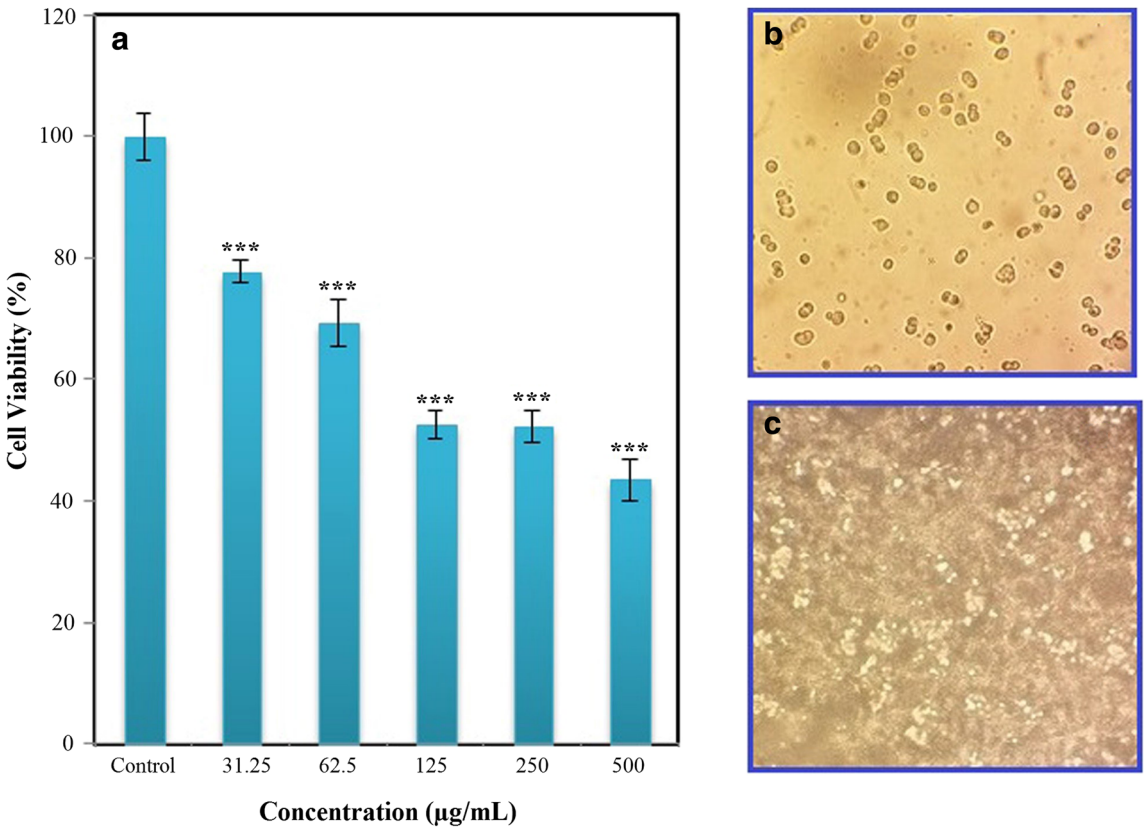

Fig. 9 **a** MTT cell viability assay of synthesized ZnO-NPs on HT-29 cancer cell line measured at 24 h; morphology of cells **b** before treatment and **c** after treatment with 500 µg/mL of synthesized ZnO-NPs at 600 °C

Thus, the A_1 (TO) mode vibrational activity was observed at 380 cm^{-1}, while the E_1 (TO) mode was discovered at 400 cm^{-1} and the E_1 (LO) mode appeared at 585 cm^{-1}. The highest intensity for the E_2 mode was observed at 441 cm^{-1}, representing a clear characteristic of crystallinity in the structure of the synthesized ZnO nanoparticles [26]. Also, the hexagonal structure of synthesized ZnO-NPs was determined through the PXRD and FESM results.

FT-IR spectrum of the synthesized ZnO-NPs (600 °C) has disclosed a series of absorption peaks from 400 to 4000 cm^{-1} (Fig. 8). The band at 459 cm^{-1} is assigned to the characteristic vibrational modes of Zn–O bonding, confirming the presence of ZnO-NPs. The broad band at 3442 cm^{-1} is attributed to the O–H stretching mode of water. Finally, the observed peaks at 1636 and 1386 cm^{-1} are related to the asymmetrical and symmetrical stretching of the carboxylate group, respectively [27].

The cytotoxic activity of ZnO-NPs on HT-29 cancer cell line was surveyed through MTT assay (Fig. 9a). This method is based on converting solvable tetrazolium salt (pink) to unsolvable formazan (purple) by the mitochondria of living cells. In this test, cancer cells were treated with the synthesized nanoparticles (500, 250, 125, 62.5, and 13.25 μg/mL, separately). According to the results, with elevation of the concentration of ZnO-NPs, the percentage of living cells decreased significantly compared to the control ($*p < 0.001$), where half of the cells died at concentrations above 125 μg/mL (IC_{50} = 262.78 μg/mL). Figures 8c and 9b display the morphology of HT-29 cells before and after the treatment with 500 μg/mL of the synthesized ZnO-NPs at 24 h.

In general, the physicochemical properties of nanoparticles including size, surface, and shape can extremely affect their toxicity [28]. Recently, scientists have become interested in the mechanism of zinc toxicity against cancerous and normal cell lines. John et al. have reported that the toxicity of Zn against colon cell line is related to ceasing the cell cycle through the ERK signal pathway (HT-29), activation of JNK (HCT-116 and SW620), and excessive expression of p38 (SW620) [29]. Other studies have stated that the reason behind Zn toxicity could be its accumulation in the cell cytoplasm, whereby cell death is induced via the activation of caspase-related apoptosis [30, 31]. In this work, synthesized zinc oxide nanoparticles indicated significant toxicity effects in comparison to the control. This study is compatible with Salari et al.'s research who reported the cell toxicity of ZnO-NPs on colon cancer cells. Their synthesized nanoparticles were spherical shaped with sizes of 30–80 nm [4]. This issue clearly illustrates the toxicity of ZnO nanoparticles against cancer cell lines.

4 Conclusion

In recent years, the production of nanoparticles has obtained a special position in studies using the principles of green chemistry. Various types of biological systems such as microorganisms, diatoms, and optical eukaryotes have been employed to investigate their abilities in electron donation and synthesis of nanoparticles. Meanwhile, plants and crops have been especially considered as cheap and renewable resources for the production of bio-nanomaterials. In this research, ZnO-NPs were synthesized through utilization of *S. persica* aqueous extract. The spectral studies including UV-Vis, PXRD, FT-IR, DLS, Raman, and FESEM indicated that the synthesized nanoparticles are uniform and hexagonal in shape with an average particle size of 60–130 nm. The examination regarding the toxicity of synthesized nanoparticles suggested that this effect is dependent on the concentration of nanoparticles.

References

1. Huang, K., Ma, H., Liu, J., Huo, S., Kumar, A., Wei, T., Zhang, X., Jin, S., Gan, Y., Wang, P. C., He, S., Zhang, X., & Liang, X. J. (2012). Size-dependent localization and penetration of ultrasmall gold nanoparticles in cancer cells, multicellular spheroids, and tumors *in vivo*. *ACS Nano, 6*, 4483–4493.
2. Bisht G., Rayamajhi S. (2016). ZnO nanoparticles: a promising anticancer agent. *Nanobiomedicine, 3*, 1-11.
3. Wahab, R., Siddiqui, M. A., Saquib, Q., Dwivedi, S., Ahmad, J., Musarrat, J., Al-Khedhairy, A. A., & Shin, H. S. (2014). ZnO nanoparticles induced oxidative stress and apoptosis in HepG2and MCF-7 cancer cells and their antibacterial activity. *Colloids and Surfaces. B, Biointerfaces, 117*, 267–276.
4. Salari, Z., Ameri, A., Forootanfar, H., Adeli-Sardou, M., Jafari, M., Mehrabani, M., & Shakibaie, M. (2017). Microwave-assisted biosynthesis of zinc nanoparticles and their cytotoxic and antioxidant activity. *Journal of Trace Elements in Medicine and Biology, 39*, 116–123.
5. Miri, A., Sarani, M., Rezazade Bazaz, M., & Darroudi, M. (2015). Plant-mediated biosynthesis of silver nanoparticles using *Prosopis farcta* extract and its antibacterial properties. *Spectrochimica Acta. Part A, Molecular and Biomolecular Spectroscopy, 141*, 287–291.
6. Khatami, M., Alijani, H. Q., Nejad, M. S., & Varma, R. S. (2018). Core@shell nanoparticles: greener synthesis using natural plant products. *Applied Sciences, 8*, 411.
7. Miri, A., Darroudi, M., Entezari, R., & Sarani, M. (2018). Biosynthesis of gold nanoparticles using *Prosopis farcta* extract and its in vitro toxicity on colon cancer cells. *Research on Chemical Intermediates, 44*, 3169–3177.
8. Khatami, M., Alijani, H. Q., & Sharifi, I. (2018). Biosynthesis of bimetallic and core shell nanoparticles: their biomedical applications: a review. *IET Nanobiotechnol, 12*, 879–887.
9. Miri, A., Dorani, N., Darroudi, M., & Sarani, M. (2016). Green synthesis of silver nanoparticles using *Salvadora persica* L. and its antibacterial activity. *Cellular and Molecular Biology, 62*, 46–50.
10. Khatami, M., Heli, H., Jahani, P. M., Azizi, H., & Nobre, M. A. L. (2017). Copper/copper oxide nanoparticles synthesis using *Stachys lavandulifolia* and its antibacterial activity. *IET Nanobiotechnol, 11*, 709–713.
11. Miri, A., & Sarani, M. (2018). Biosynthesis, characterization and cytotoxic activity of CeO_2 nanoparticles. *Ceramics International, 44*, 12642–12647.

12. Arora, M., & Gupta, V. K. (2011). Phytochemical and biological studies on *Salvadora persica* wall: a review. *Pharmacologyonline, 1*, 591–601.
13. Yadav, J., Saini, S., & Kalia, A. (2005). Botanical, cytological, phytochemical and pharmacognostical studies on *Salvadora* species. *Journal of Medicinal Plant Sciences, 2*, 231–238.
14. Halawany, H. S. (2012). A review on miswak (*Salvadora persica*) and its effect on various aspects of oral health. *Saudi Dental Journal, 24*, 63–69.
15. Hafiz, U., Hafiz, A., Momin, A., & Dawoodbhoy, R. (2016). Effects of *Salvadora persica* on oral health: a birds eye view. *IJPCDR, 3*, 271–276.
16. Halib, N., Nuairy, N. B., Ramli, H., Ahmad, I., Othman, N. K., Salleh, S. M., & Bakarudin, S. B. (2017). Preliminary assessment of *Salvadora persica* whitening effects on extracted stained teeth. *Journal of Applied Pharmaceutical Science, 7*, 121–125.
17. Deswal, H., Singh, Y., Grover, H. S., Bhardwaj, A., & Verma, S. (2016). Miswak as an alternative treatment modality in medicine and dentistry: a review. *Innovare Journal of Life Sciences, 4*(2), 6–8.
18. Nava, O. J., Luque, P. A., Gómez-Gutiérrez, C. M., Vilchis-Nestor, A. R., Castro-Beltrán, A., Mota-González, M. L., & Olivase, A. (2017). Influence of *Camellia sinensis* extract on zinc oxide nanoparticle green synthesis. *Journal of Molecular Structure, 1134*, 121–125.
19. Khatami, M., Sharifi, I., Nobre, M. A. L., Zafarnia, N., & Aflatoonian, M. R. (2017). Waste-grass-mediated green synthesis of silver nanoparticles and evaluation of their anticancer, antifungal and antibacterial activity. *Green Chemistry Letters and Reviews, 11*(2), 125–134.
20. Alwan, R. M., Kadhim, Q. A., Sahan, K. M., Ali, R. A., Mahdi, R. J., Kassim, N. A., & Jassim, A. N. (2015). Synthesis of zinc oxide nanoparticles via sol-gel route and their characterization. *Nanoscience and Nanotechnology, 5*, 1–6.
21. Rajiv, P., Rajeshwari, S., & Venckatesh, R. (2013). Bio-fabrication of zinc oxide nanoparticles using leaf extract of *Parthenium hysterophorus* L. and its size-dependent antifungal activity against plant fungal pathogens. *Spectrochimica Acta. Part A, Molecular and Biomolecular Spectroscopy, 112*, 384–387.
22. Khorsand Zak, A., Yousefi, R., Majid, W. H. A., & Muhamad, M. R. (2012). Facile synthesis and X-ray peak broadening studies of $Zn_{1-x}Mg_xO$ nanoparticles. *Ceramics International, 38*, 2059–2064.
23. Khorsand Zak, A., Abd Majid, W. H., Mahmoudian, M. R., Darroudi, M., & Yousefi, R. (2013). Starch-stabilized synthesis of ZnO nanopowders at low temperature and optical properties study. *Advanced Powder Technology, 24*, 618–624.
24. Kundu, S. (2014). A facile route for the formation of shape-selective ZnO nanoarchitectures with superior photo-catalytic activity. *Colloids and Surfaces A: Physicochemical and Engineering Aspects, 446*, 199–212.
25. Romčević, N., Kostić, R., Romčević, M., Hadˇzić, B., Kuryliszyn-Kudelska, I., Dobrowolski, W., Narkiewicz, U., & Sibera, D. (2008). Raman scattering from ZnO(Fe) nanoparticles. *Acta Physica Polonica A, 114*, 1323–1328.
26. Jaramillo, A. F., Baez-Cruz, R., Montoya, L. F., Medinam, C., Pérez-Tijerina, E., Salazar, F., Rojas, D., & Melendrez, M. F. (2017). Estimation of the surface interaction mechanism of ZnO nanoparticles modified with organosilane groups by Raman spectroscopy. *Ceramics International, 43*, 11838–11847.
27. Pavithra, N. S., Lingaraju, K., Raghu, G. K., & Nagaraju, G. (2017). *Citrus maxima* (pomelo) juice mediated eco-friendly synthesis of ZnO nanoparticles: applications to photocatalytic, electrochemical sensor and antibacterial activities. *Spectrochimica Acta. Part A, Molecular and Biomolecular Spectroscopy, 185*, 11–19.
28. Moezzi, A., McDonagh, A. M., & Cortie, M. B. (2012). Zinc oxide particles: synthesis, properties and applications. *Chemical Engineering Journal, 185-186*, 1–22.
29. John, S., Briatka, T., & Rudolf, E. (2011). Diverse sensitivity of cells representing various stages of colon carcinogenesis to increased extracellular zinc: implications for zinc chemoprevention. *Oncology Reports, 25*, 769–780.
30. Lopez, V., Foolad, F., & Kellher, S. L. (2011). ZnT_2-overexpression represses the cytotoxic effects of zinc hyper-accumulation in malignant metal lothionein-null T47D breast tumor cells. *Cancer Letters, 304*, 41–51.
31. Rudolf, E., & Cervinka, M. (2011). Stress responses of human dermal fibroblasts exposed to zinc pyrithione. *Toxicology Letters, 204*, 164–173.